Electronic Supplementary Material (ESI) for Inorganic Chemistry Frontiers.
This journal is © the Partner Organisations 2024

Calculation details

The electronic structure calculations exclusively employed the Dmol^3 software[1]. Describing the exchange-correlation energy of electrons, we utilized the Perdew-Burke-Ernzernhof (PBE) type of generalized gradient approximation (GGA) functional[2]. Employing a double numeric plus polarization (DNP) basis set[3], the electronic structure was effectively characterized. Monkhorst-Pack k-point grids[4] were employed for Brillouin zone sampling. For periodic structures, the k-point sampling interval was set to 0.023 Å^{-1}. A vacuum layer of 15 Å was introduced between the slabs to minimize interactions, providing accurate adsorption energy. Grimme's dispersion-corrected density functional theory (DFT-D)[5] was applied to account for van der Waals forces in the system.

The orbital cutoff radius was set to 5.0 Å, and Gaussian-like smearing with a width of 0.005 Ha was used for electronic-level thermal occupation[6]. The entropy correction term arising from thermal occupation was subtracted during total energy calculations. The system had a zero magnetic moment, and spin polarization was not considered. The convergence criterion for electronic self-consistent interactions was set to 1×10^{-6} Ha. During structure optimization, the maximum force convergence criterion was set to 0.002 Ha·Å^{-1}, and the total energy difference was required to be less than 1×10^{-5} Ha. Periodic slab structures were employed to calculate the adsorption energy of glycerol and water molecules, comprising a total of 64 magnesium atoms in 4 layers. Unspecified parameters did not significantly impact the conclusions drawn in this work.

Adsorption energy (E_{ads}) was computed using the formula[7]:

$$E_{ads}=E_{(X+slab)}-E_{(slab)}-E_{(X)}$$

Here, $E_{(X+slab)}$ is the total energy of X adsorbed slab, $E_{(slab)}$ is the energy of the clean slab, and $E_{(X)}$ is the energy of the adsorption species X.

Similarly, binding energy (E_{bin}) was calculated using the formula:

$$E_{bin}=E_{(Y+Z)}-E_{(Y)}-E_{(Z)}$$

Here, $E_{(Y+Z)}$ represents the total energy of the Y and Z bound species, and $E_{(Y)}$ and $E_{(Z)}$ are the energies of the respective adsorption species Y and Z.

Molecular dynamics (MD) studies were conducted using Large-scale Atomic/Molecular Massively Parallel Simulator (Lammps) software[8] with an transferable intermolecular potential 3-point model combined with the Harvard molecular mechanics (CHARMM22) hybrid force field to describe the system[9,10]. The MD simulations were performed in a three-dimensional box with periodic boundary conditions, while the surface atoms were kept fixed. The model included 6 layers of magnesium surface, consisting of a total of 288 magnesium atoms, as well as 1100 water molecules, 5 units of $MgCl_2$, and 10 glycerol molecules in the electrolyte region. The simulations were carried out using the canonical ensemble (NVT). Prior to the formal simulations, the system was pre-equilibrated using the Nose-Hoover method[11,12] at a temperature of 700 K for 100 ps to obtain a reasonable initial configuration. Subsequently, the Nose-Hoover thermostat method was employed to perform a 5 ns simulation at a temperature of 300 K with a time step of 0.5 fs. Finally, the simulation trajectories were visualized using the OVITO program[13].

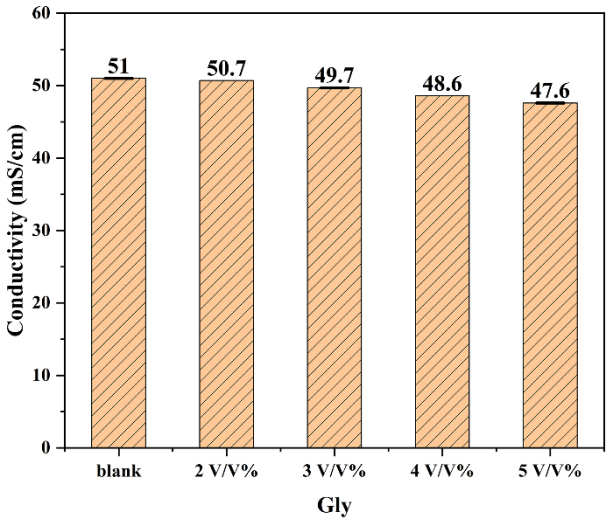

Fig. S1 Ionic conductivity of different electrolytes.

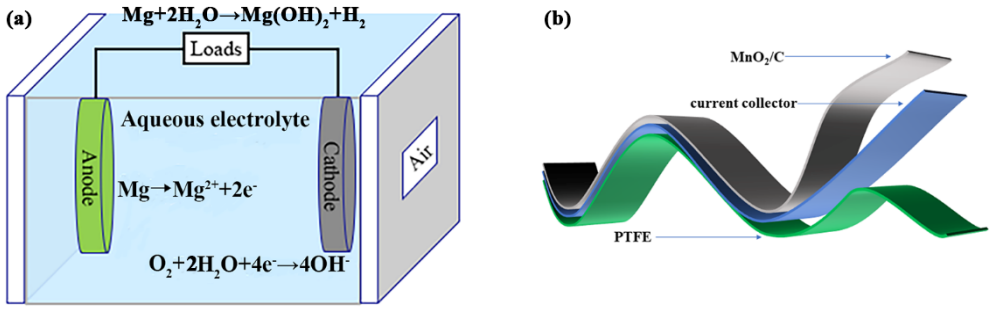

Fig. S2 Schematic diagram of (a) Mg-air battery; (b) cathode.

The cathode structure consists of a hydrophobic breathable layer, a current collector, and a catalytic layer. The composition of the hydrophobic breathable layer is PTFE, the current collector is made of stainless steel mesh, and the catalytic layer contains a mass ratio of 7:3 of MnO_2 and C, with a loading of 15mg/cm^2.

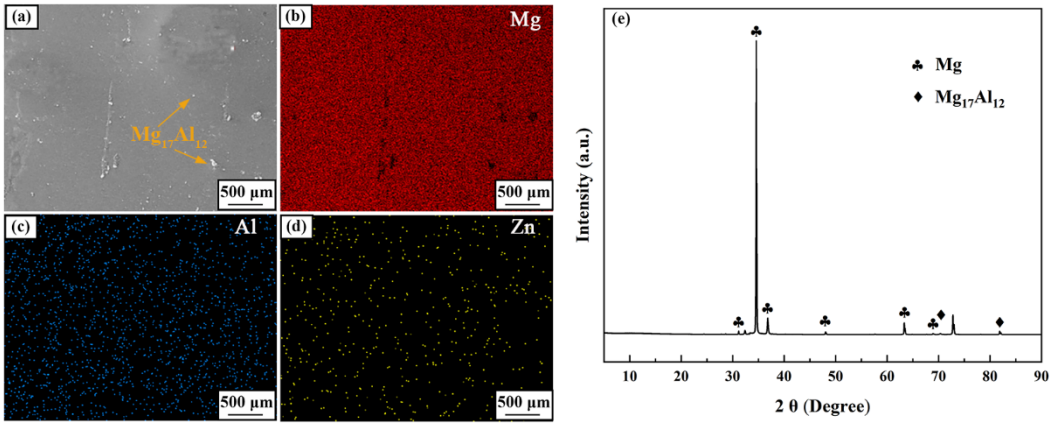

Fig. S3 AZ31 Mg alloy (a) surface morphology; (b-d) EDS energy spectrum analysis; (e) XRD analysis.

Table S1 Composition of AZ31 detected by ICP-AES.

Alloy	Actual constituent(wt.%)				
	Mg	Al	Zn	Mn	Si
AZ31	Bal.	3.05	0.97	0.28	0.08

Table S2 Charge transfer of three models calculated through Mullikens charge population analysis.

model	Mg-glycerol-parallel	Mg-glycerol-vertical	Mg-water
Electron loss in magnesium slab	0.122	0.076	0.080

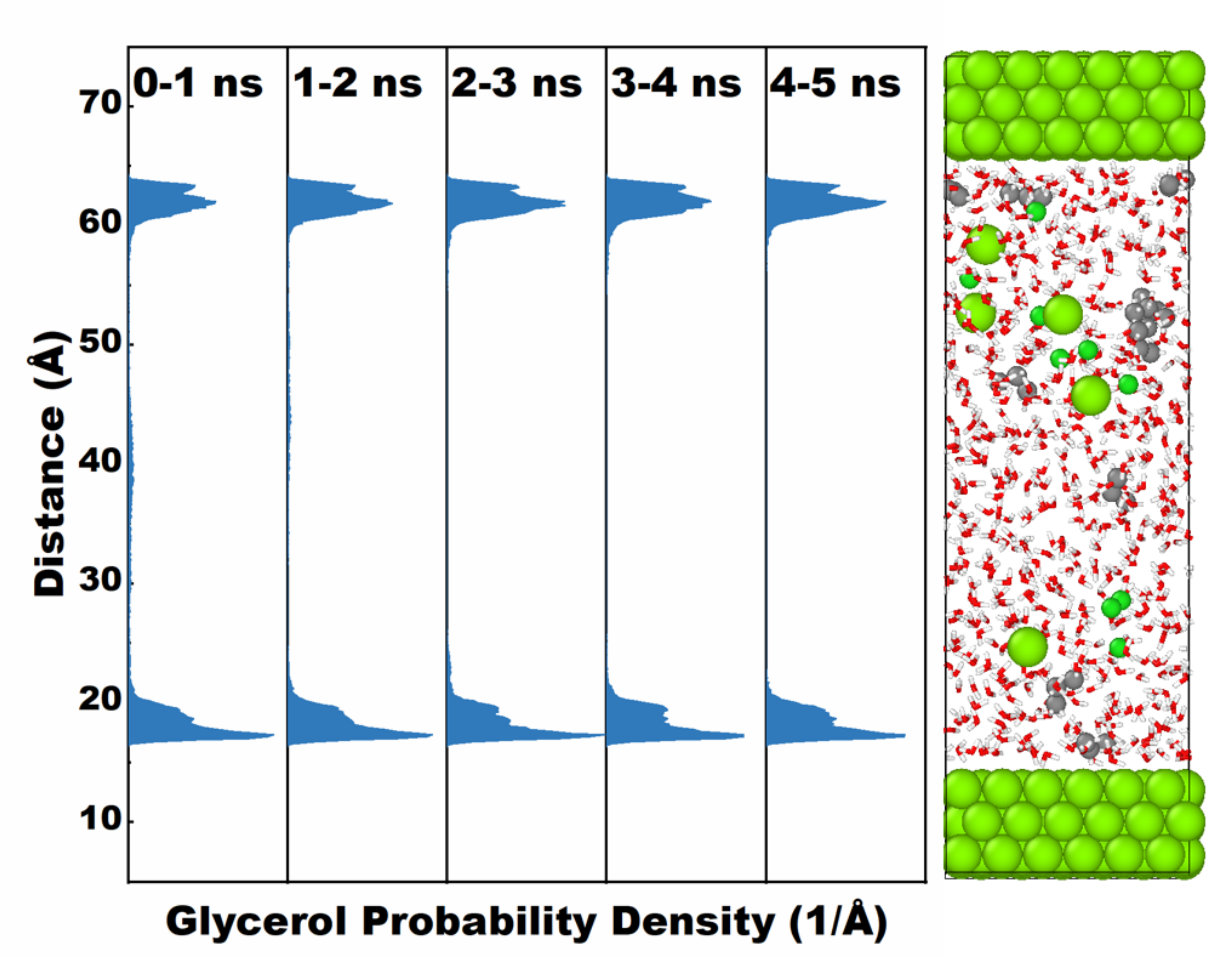

Fig. S4 Probability density evolution of glycerol molecules over time along with the electrolyte model. In the electrolyte model depicted on the right, green represents Mg atoms, dark green signifies Cl atoms, red denotes O atoms, white represents H atoms, and black indicates C atoms. The distance in the z-direction of the model corresponds to the probability density plot.

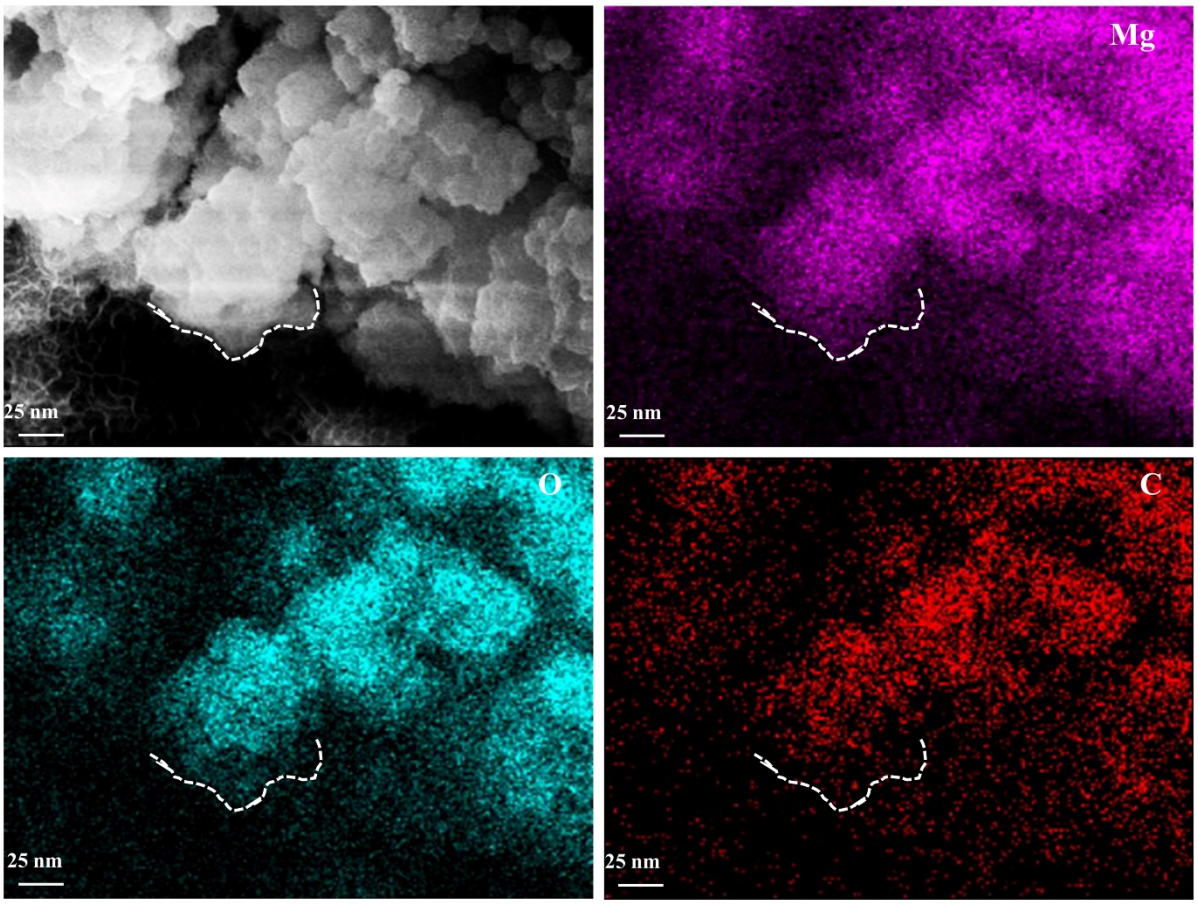

Fig. S5 Image and corresponding elemental mapping of the discharged product layer after the addition of 3V/V% Gly.

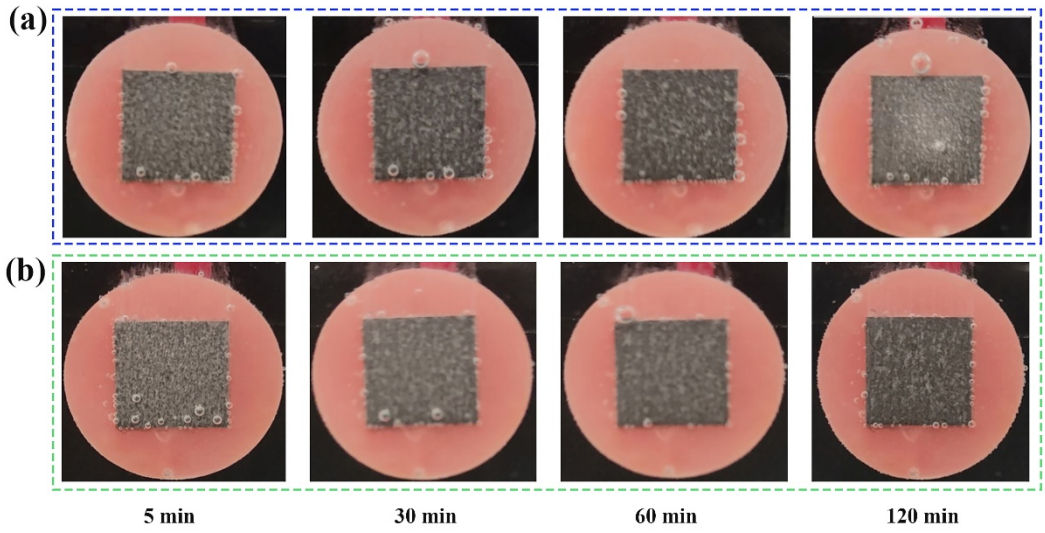

Fig. S6. Morphologies of anodes in electrolytes of different durations observed using in situ endoscopy: (a) blank,

(b) 3V/V% Gly.

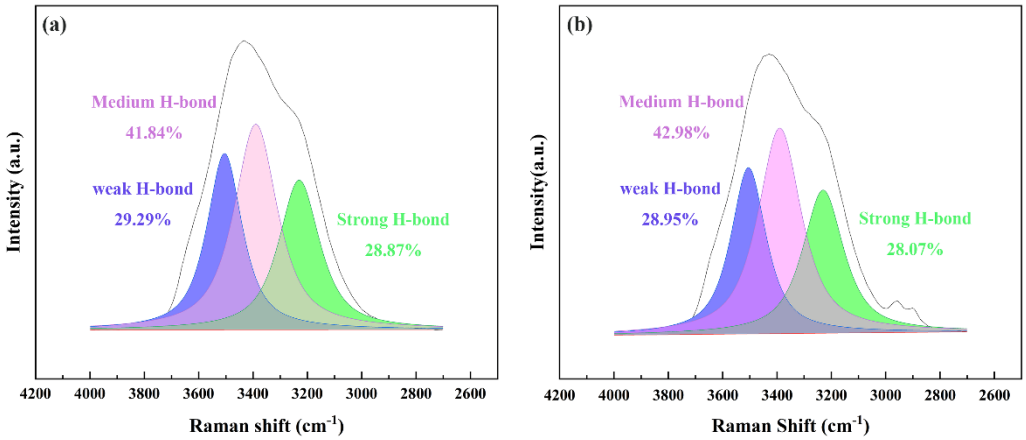

Fig. S7. The Raman of (a) blank, (b) 3V/V% Gly electrolytes were fitted with three peaks representing the O–H stretching vibration of H_2O in weak, medium, strong H-bond state.

Table S3 Fitting results of dynamic potential curves of AZ31 electrode in different electrolytes

Sample	E_{corr}(V)	I_{corr}(A cm^{-2})	β_a(mV)	β_c(mV)
blank	–1.42	6.27×10^{-5}	70.82	170.18
3V/V%	–1.47	3.88×10^{-5}	64.42	129.69

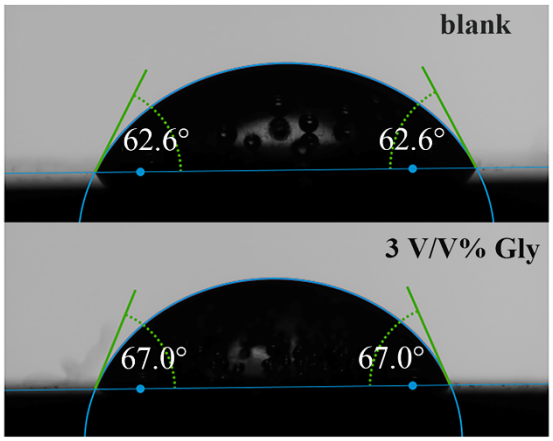

Fig. S8. Contact angle between different electrolytes and magnesium substrate.

References:

1 B. Delley, From Molecules to Solids with the DMol3 Approach, *J. Chem. Phys,* 2000, **113**, 7756–7764.

2 J. P. Perdew, K. Burke and M. Ernzerhof, Generalized Gradient Approximation Made Simple. *Phys. Rev. Lett.* 1996, **77**, 3865–3868.

3 B. Delley, An All-electron Numerical Method for Solving the Local Density Functional for Polyatomic Molecules, *J. Chem. Phys.,* 1990, **92**, 508–517.

4 H. J. Monkhorst, J. D. Pack, Special Points for Brillouin-Zone Integrations, *Phys. Rev. B,* 1976, **13** , 5188–5192.

5 S. Grimme, Semiempirical GGA-type density functional constructed with a long-range dispersion correction, *J. Comput. Chem,.* 2006, **27**, 1787–1799.

6 N. Marzari, D. Vanderbilt and M. C. Payne, Ensemble Density-Functional Theory for Ab Initio Molecular Dynamics of Metals and Finite-Temperature Insulators, *Phys. Rev. Lett,* 1997, **79**, 1337–1340.

7 X. Yin, H. Wang and E.-H. Han, Effects of Solvation and Applied Potential on the Adsorption Behaviors of H, O, OH and H2O on Fe(110) Surface, *Surf. Sci.,* 2020, **691**, 121504.

8 S. Plimpton, Fast Parallel Algorithms for Short-Range Molecular Dynamics, *J. Comput. Phys.,* 1995, ***117*,** 1–19.

9 A. D. MacKerell, D. Bashford and M. Bellott, All-Atom Empirical Potential for Molecular Modeling and Dynamics Studies of Proteins, *J. Phys. Chem. B,* 1998, **102**, 3586–3616.

10 H. Wang, H. Yuan, J. Wang, E. Zhang, M. Bai, Y. Sun, J. Wang, S. Zhu, Y. Zheng and S. Guan, Influence of the Second Phase on Protein Adsorption on Biodegradable Mg Alloys' Surfaces: Comparative Experimental and Molecular Dynamics Simulation Studies, *Acta Biomater.,* 2021, **129**, 323–332.

11 W. G. Hoover, Canonical Dynamics: Equilibrium Phase-Space Distributions, *Phys. Rev. A,* 1985, **31**, 1695–1697.

12 S. Nosé, A Unified Formulation of the Constant Temperature Molecular Dynamics Methods, *J. Chem. Phys.,* 1984, **81**, 511–519.

13 A. Stukowski, Visualization and Analysis of Atomistic Simulation Data with OVITO–the Open Visualization Tool, *Model. Simul. Mater. Sci. Eng.* 2010, **18**, 015012.